

Optically Driven Magnetic Phase Transition of Monolayer RuCl₃

Yingzhen Tian^{1*}, Weiwei Gao^{2*}, Erik A. Henriksen¹, James R. Chelikowsky^{2,3,4}, Li Yang¹

1. Department of Physics and Institute of Materials Science and Engineering, Washington University, St. Louis, MO 63130, USA

2. Center for Computational Materials, Institute for Computational Engineering and Sciences, The University of Texas at Austin, Austin, TX 78712 USA

3. Department of Physics, The University of Texas at Austin, Austin, TX 78712 USA

4. Department of Chemical Engineering, The University of Texas at Austin, Austin, TX 78712 USA

ABSTRACT: Strong light-matter interactions within nanoscale structures offer the possibility of optically controlling material properties. Motivated by the recent discovery of intrinsic long-range magnetic order in two-dimensional materials, which allows for the creation of novel magnetic devices of unprecedented small size, we predict that light can couple with magnetism and efficiently tune magnetic orders of monolayer ruthenium trichloride (RuCl₃). First-principles calculations show that both free carriers and optically excited electron-hole pairs can switch monolayer RuCl₃ from the proximate spin-liquid phase to a stable ferromagnetic phase. Specifically, a moderate electron-hole pair density (on the order of $1 \times 10^{13} \text{ cm}^{-2}$) can significantly stabilize the ferromagnetic phase by 10 meV/f.u. in comparison to the zigzag phase, so that the predicted ferromagnetism can be driven by optical pumping experiments. Analysis shows that this magnetic phase transition is driven by a combined effect of doping-induced lattice strain and itinerant ferromagnetism. According to the Ising-model calculation, we find that the Curie temperature of the ferromagnetic phase can be increased significantly by raising carrier or electron-hole pair density. This enhanced opto-magnetic effect opens new opportunities to manipulate two-dimensional magnetism through non-contact, optical approaches.

1. INTRODUCTION

Since the discovery of graphene, new classes of atomically thin materials, such as transition metal dichalcogenides (TMDs), black phosphorus, and many others, have been synthesized. Such materials display a wide range of remarkable mechanical, optical, and electronic properties, which only appear in their two-dimensional (2D) forms. Particular efforts have been invested in realizing ferromagnetism in 2D materials, such as applying an external strain¹⁻², doping³, introducing adatoms⁴, or using proximity effects⁵. Recently, intrinsic ferromagnetism that persists in the 2D limit was observed in monolayer CrI₃⁶, monolayer and few-layer CrXTe₃ (X=Ge, Si)⁷⁻⁸, VSe₂⁹, and Fe₃GeTe₂¹⁰ etc.¹¹⁻¹² These materials offer new opportunities for studying spin physics in low dimensions, and for designing spintronic devices of unprecedentedly small size¹²⁻¹³. Following these seminal discoveries, several groups independently demonstrated the tunability of magnetic orders of 2D systems¹⁴⁻¹⁵. For example, they found that the interlayer coupling of bilayer CrI₃ can be reversibly tuned from the antiferromagnetic (AFM) to the ferromagnetic (FM) phase by changing the free-carrier concentration via gate voltage¹⁴⁻¹⁵.

Beyond mechanical strain, chemical doping, and electrostatic gating, optically tuning material properties is highly preferable as no contacts are involved. The enhanced light-matter interactions in layered van der Waals (vdW) materials strengthen the possibility to optically control material

properties.¹⁶⁻¹⁷ Optical pumping induced structural phase transitions in TMDs, photoinduced insulator-to-metal phase transition in VO₂ thin film¹⁸⁻²⁰, optically tunable magnetism²¹⁻²³, and light-induced superconductivity in cuprates²⁴ are examples of light controlled properties in materials. Enhanced opto-piezoelectric effects have been predicted in monolayer group IV-VI materials as well.²⁵ The recent breakthrough in 2D magnetism suggests a search for optically tunable magnetism in 2D systems.

Among magnetic vdW materials, α -RuCl₃ is a good candidate to search for opto-magnetic effects. Similar to CrXTe₃ (X=Ge, Si) and CrI₃, α -RuCl₃ is a layered material with weak vdW interactions between layers. First-principles calculations show that α -RuCl₃ has small cleavage energy, and monolayer (and few-layer) RuCl₃ have recently been obtained through mechanical exfoliation in experiments²⁶⁻²⁸. Bulk α -RuCl₃ displays an in-plane “zigzag” antiferromagnetic (zigzag AFM) order²⁹ where the magnetic moments of Ru³⁺ ions align ferromagnetically with other Ru³⁺ in the same zigzag chain, and antiferromagnetically with those in neighboring zigzag chains. Recent research has shown that α -RuCl₃ is a possible system for studying the Kitaev model. This model is exactly solvable and hosts rich and exotic magnetic phenomena, including bond-dependent exchange coupling, rich quantum spin liquid phases and fractional excitations³⁰. These interesting magnetic properties can possibly be retained in the monolayer limit, given that the interlayer exchange coupling is only a few percent of the intralayer exchange coupling according to *ab initio* calculations³¹, and the anisotropic alignment of magnetic moments of Ru ions provides the necessary condition for long-range 2D magnetic order, according to the Mermin-Wagner theorem^{7,32}.

Here, we show that unipolar doping and optical electron-hole (*e-h*) bipolar doping can be efficient approaches to switch the ground state of monolayer RuCl₃ from the proximate spin-liquid phase to the FM order. The critical carrier densities for realizing this magnetic phase transition are moderate, on the order of 10¹³ cm⁻² for electrons, holes, and photoexcited *e-h* pairs. As a result, 2D ferromagnetism can be turned on/off by electrostatic gating and, more interestingly, by optical pumping with a practical *e-h* density. Moreover, we reveal that the electron-doping-driven FM order is mainly from lattice distortions, while the hole- and *e-h* pair-driven FM orders are mainly from itinerant electrons. The estimated Curie temperature based on an Ising model is above the liquid-nitrogen temperature and can be further increased by higher carrier/*e-h* pair densities.

2. RESULTS AND DISCUSSION

2.1. Structural and magnetic properties

Monolayer RuCl₃ has a similar structure as monolayer chromium trihalides, such as the ferromagnetic CrI₃. As shown in Figures 1 (a) and (b), Ru³⁺ ions bond with six nearest-neighbor Cl¹⁻ ions, forming edge-sharing RuCl₆ octahedra, which show trigonal distortions from the regular octahedron^{26,29}. The zigzag AFM spin configuration enlarges the hexagonal unit cell to be an orthorhombic supercell containing 16 atoms, as shown in Figure 1 (b). This supercell is used for our calculations and discussions unless otherwise stated.

Depending on the ratio of the Heisenberg exchange and Kitaev interaction, the solution of the Heisenberg-Kitaev model³³ corresponds to four phases with long-range magnetic orders: the zigzag, Neel, Stripy, and ferromagnetic phases in intrinsic monolayer RuCl₃. To elucidate the spin configurations of these phases, we schematically plot the arrangement of the local magnetic moments of Ru³⁺ ions with colored arrows in Figure 1 (c). Using an effective Hubbard $U_{\text{eff}}=U-J$ of 2 eV^{31,34}, our *ab initio* density functional theory (DFT) calculations reveal that the zigzag AFM phase has the lowest energy among four magnetic phases. The competing FM phase has a slightly higher energy of ~ 0.05 meV per f.u. (formula unit) relative to the zigzag phase. The energies of the Neel and stripy AFM phases are notably higher (more than 4.6 meV/f.u.) than the other two. These relative energies are summarized in Figure 1 (c) and agree well with a previous work³⁴. By checking the effects of Hubbard U_{eff} value on our calculations, we find the energy ordering of four magnetic phases (i.e., $E(\text{Zigzag}) \approx$

$E(\text{FM}) < E(\text{stripy}) < E(\text{Neel})$) remain the same for the range of U_{eff} from 2 to 5 eV (See Figure S1 in Supporting Information).

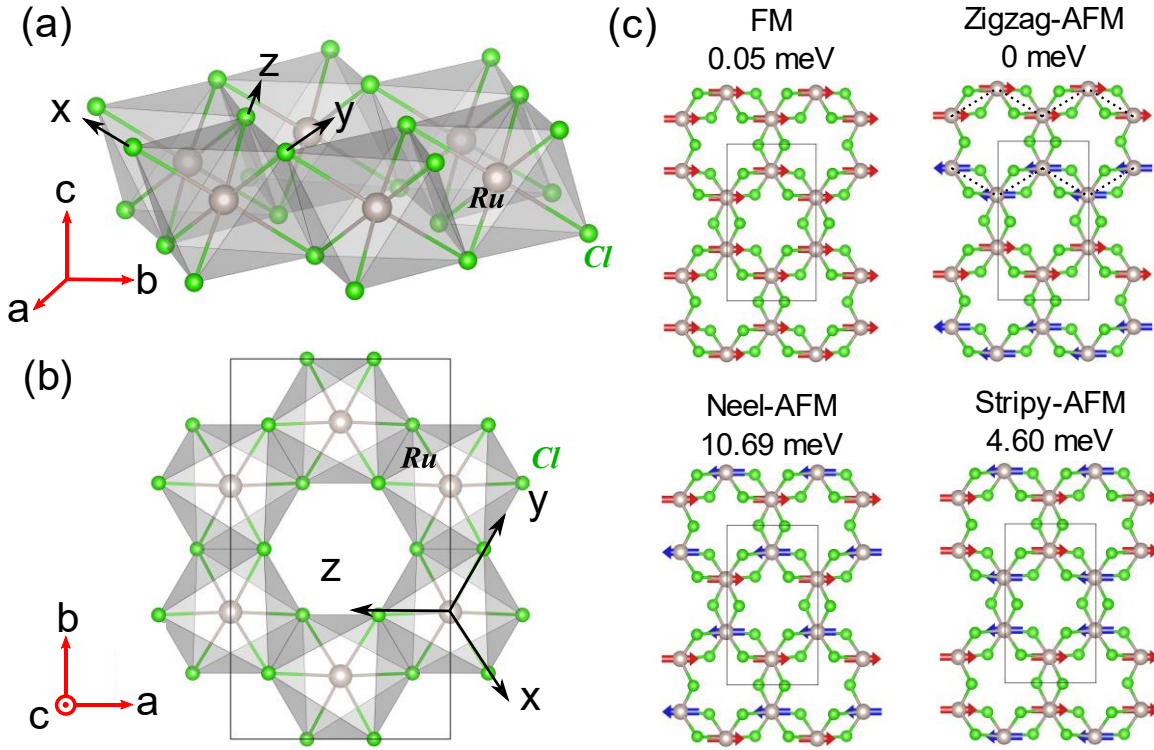


Figure 1 (a) and (b) Top and side views of the crystal structure of monolayer RuCl₃. The rectangle shows the 16-atom supercell used in our calculations. (c) Schematic plots of the supercell and spin configurations of four magnetic orders, i.e., the ferromagnetic, zigzag AFM, Neel-AFM, and stripy AFM phases. The zigzag chains in zigzag-AFM phase are shown as dashed lines. The relative energies (per formula unit) to the zigzag AFM state are presented as well.

Although our calculation shows that the zigzag AFM phase has the lowest energy among four spin configurations, the small energy difference between the zigzag AFM and FM phases is only 0.05 meV/f.u., within the accuracy of the DFT+U approach. This indicates that the zigzag AFM phase and FM phase are nearly degenerate in the undoped situation. Debates on the magnetic order of monolayer RuCl₃ also exists in the literature. For example, Iyikanat et al. predicted that the zigzag AFM phase is the ground state³⁴, while Sarikurt et al. predicted that the competing FM phase is the ground state³⁵. Nevertheless, both works show the energy difference between the zigzag AFM and FM phases is small (less than 1.2 meV/f.u.). The discrepancy between different calculations is due to the enhanced magnetic frustration in single-layer RuCl₃, as shown in a recent Raman scattering experiment²⁸. In particular, as the dimension of RuCl₃ changes from bulk to monolayer, the experiment²⁸ shows the increasingly strong phonon-magnetic scattering, a hallmark of quantum spin liquids. These experimental and theoretical evidences support that the undoped monolayer RuCl₃ is in a proximate quantum spin-liquid phase.

2.2. Effects of unipolar doping

We consider the role of unipolar doping on the magnetic order of monolayer RuCl₃. The doped free carriers are introduced by the electrostatic doping approach, which has been widely applied to

studying free-carrier doping effects on magnetism³⁶⁻³⁸ and realized by voltage gating approaches in experiments^{10, 14}. In Figure 2 (a), we present the total energies of three AFM phases (*i.e.*, zigzag, Neel, and stripy phases) relative to that of the FM phase (denoted as $E(\text{AFM})-E(\text{FM})$) under different doping densities. The Neel and stripy AFM phases always have significantly higher energies within a reasonable range of doping densities. Therefore, we focus on the competition between the FM and zigzag AFM phases.

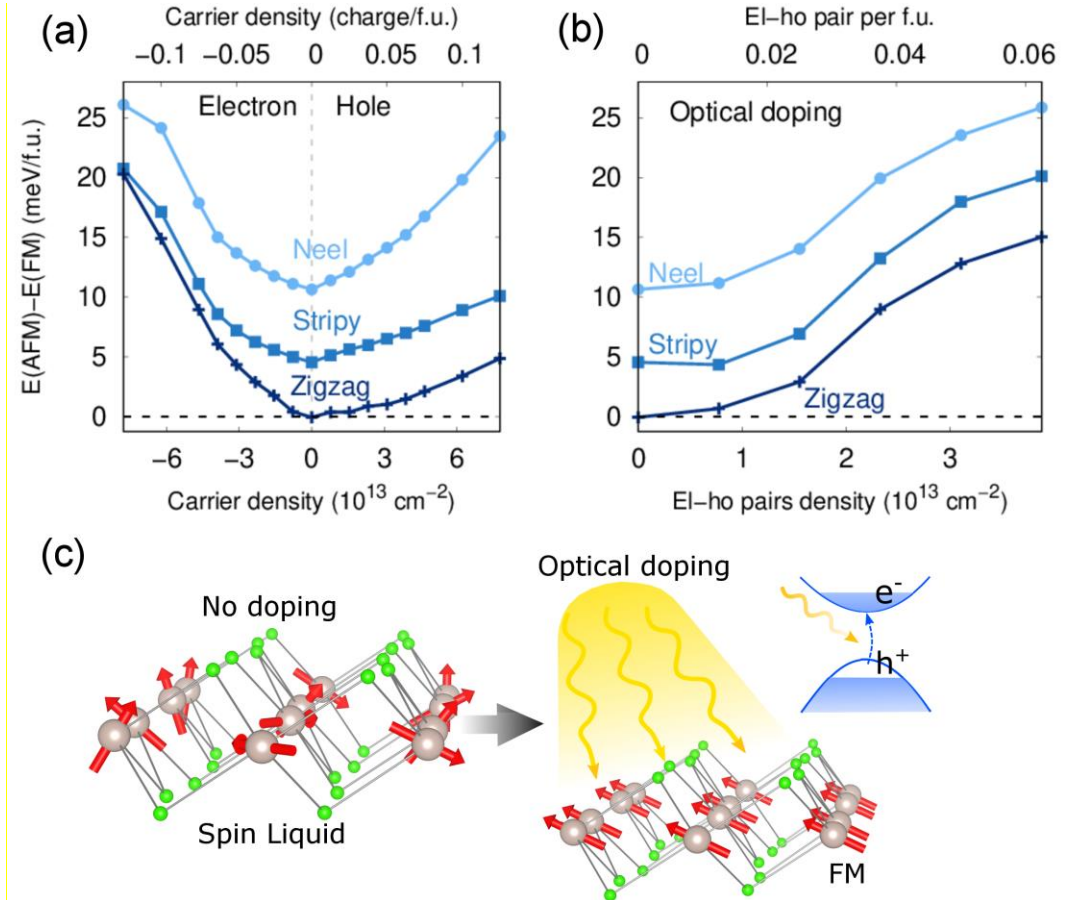


Figure 2 (a) and (b) the relative energies to the zigzag AFM phase of monolayer RuCl_3 for unipolar doping and optical $e-h$ doping, respectively. (c) Schematically plot the optically tunable 2D magnetism in RuCl_3 .

As shown in Figure 2 (a), $E(\text{Zigzag})-E(\text{FM})$ changes from a small negative value to positive as the concentration of free carriers (either electrons or holes) increases. This suggests that doped monolayer RuCl_3 energetically prefers the FM phase over the zigzag AFM phase. For example, to induce an $E(\text{Zigzag})-E(\text{FM}) > 5 \text{ meV/f.u.}$, one needs to dope around $4 \times 10^{13} \text{ cm}^{-2}$ electrons or $8 \times 10^{13} \text{ cm}^{-2}$ holes. Such carrier densities are comparable with the critical density ($2.6 \times 10^{13} \text{ cm}^{-2}$) for the doping-induced magnetic phase transition of bilayer CrI_3 ¹⁴⁻¹⁵. Particularly, the energy difference between the zigzag AFM and FM phases can be increased to around 20 meV/f.u. with an electron doping density of $7.7 \times 10^{13} \text{ cm}^{-2}$. For reference, a recently experimentally confirmed room-temperature 2D magnet VSe_2 displays an energy difference of 24 meV/f.u. between the FM and AFM orders by first-principles calculations¹. Accordingly, we expect that unipolar doping can drive the ground state from the nearly degenerate magnetic orders to the FM order. Finally, we have checked the doping and screening impacts on the effective onsite Coulomb interaction U . We found that the variation of U between doping

densities of 0.20 electron/supercell and 0.20 hole/supercell is about 0.2 eV. Therefore, this small variation of U will not change the above conclusion.

2.3. Effects of optical doping

An important character of RuCl_3 is that, unlike bilayer CrI_3 ¹⁴ and monolayer GaSe ³⁶, in which only one type of free carriers can tune the magnetic order, monolayer RuCl_3 transits to the FM phase by either electron doping or hole doping. This indicates a possible optical doping effect³⁹⁻⁴¹ in which photoexcited electrons and holes are created simultaneously to drive the magnetic phase transition. To study the role of photo-excited electrons and holes, we employ a constrained DFT approximation, in which we manually change the occupation numbers of valence and conduction states to mimic the simultaneous existence of photo-excited electrons and holes. This approach has successfully been applied to examine excited-state structures of defects⁴²⁻⁴³ and photo-induced structural changes (perovskites and monolayer SnSe)^{25, 44}. The effects of optical doping are modeled with 64-atom supercells.

Figure 2 (b) illustrates the total energies of three AFM phases relative to the FM phase (denoted as $E(\text{AFM})-E(\text{FM})$) as a function of optical doping. Focusing on the competition between the FM and zigzag AFM phases, $E(\text{Zigzag})-E(\text{FM})$ increases monotonically with the density of $e-h$ pairs. A significant energy difference between the FM and zigzag AFM phases of approximately 10 meV/f.u. is observed under a moderate $e-h$ pair density of $3.0 \times 10^{13} \text{ cm}^{-2}$. This suggests the possibility to tune magnetic properties of 2D RuCl_3 by non-contacting optical approaches. We plot such a photo-induced magnetic effect schematically in Figure 2 (c).

Next, we discuss the feasibility of observing photo-induced magnetic phase transition in experiments. In monolayer transition metal dichalcogenide^{41, 45}, optical pumping can generate $e-h$ pairs with densities up to 10^{14} cm^{-2} , which could be large enough to stabilize the FM phase. The photo-induced ferromagnetism can then be detected with the time-resolved magneto-optical Kerr effect, which measures magnetic responses in the timescale of femtosecond.⁴⁶⁻⁴⁷ Another way to observe the photoinduced ferromagnetism in monolayer RuCl_3 is to apply continuous light illumination, which can ensure the photo-excited carriers to reach equilibrium. This approach has been demonstrated experimentally. By using light-emitting diode, B. Náfrádi et al. demonstrate the melting of ferromagnetism in $\text{CH}_3\text{NH}_3(\text{Mn:Pb})\text{I}_3$ ²¹ due to the photo-induced carriers.

Finally, the imbalance of electron and hole concentration caused by extrinsic factors, such as deep-level defects⁴⁵, are not considered in our calculations. However, as seen in Figure 2 (a), unipolar doping also strongly favors the FM order, making our prediction robust to different concentrations of electrons and holes.

2.4. The mechanism of the doping and opto-magnetic effects

It is important to understand the mechanism of the doping-induced effect on magnetic orders. First, we realize that the structural variation induced by doping could be an important factor to favor the FM order. Doped carriers can substantially change the lattice constants of monolayer RuCl_3 , and strain is also known to impact the magnetic order^{31, 34}. Within the range of ± 0.075 electron/f.u. doping density, as shown in Figure 3 (a), the in-plane lattice constants, a and b , monotonically vary within 2%. When the type of free carriers changes from hole to electron, the in-plane strain changes from compressive to tensile. Interestingly, as shown in Figure 3 (b), if we fix the crystal structure as that of the undoped situation, electron doping does not favor the FM order. Therefore, electron doping induces a tensile strain that is crucial to favoring the FM order. On the other hand, the hole doping shrinks the in-plane lattice constants (Figure 3 (a)), and, moreover, $e-h$ optical doping does not change the lattice constants significantly, as shown in Figure 3 (c). Even if we fix the crystal structure, hole doping and

e - h optical doping still change the relative energies between the FM and zigzag AFM orderings, as shown in Figure 3 (b) and (d), indicating that they have different mechanism to prefer the FM order.

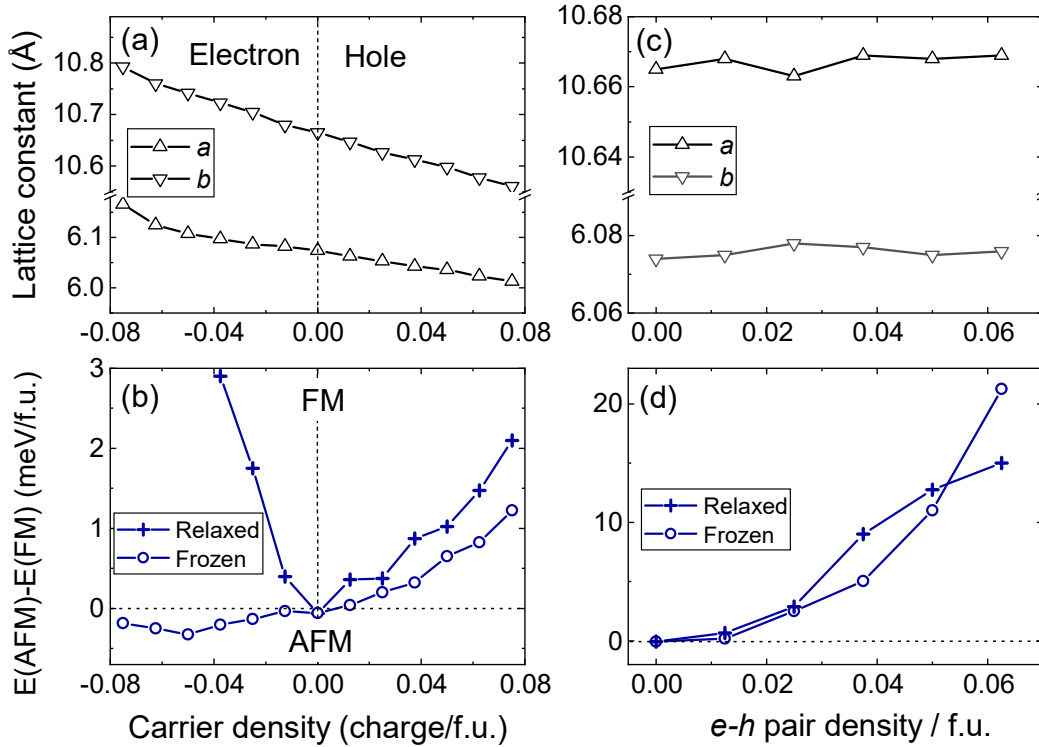


Figure 3 (a) and (c) The lattice constants of the supercell of monolayer RuCl₃ according to the unipolar and optical dopings, respectively. (b) and (d) The energy difference between the FM and zigzag AFM phases according to the unipolar and optical dopings, respectively. Results calculated with fully relaxed and frozen structures under doping are compared. Note the data points for relaxed structures (plotted with small cross) in (b) and (d) are the same as Figure 2 (a) and (b), respectively.

Many factors influence the magnetic order of solids. For doped monolayer RuCl₃, we identify that both itinerant electrons and localized magnetic moments contribute significantly to the doping induced ferromagnetism.

For the first mechanism, the itinerant magnetism, we calculated the density of state (DOS) for monolayer intrinsic RuCl₃ in a non-magnetic state. Van Hove singularities (vHSs) in the DOS appear right above and below the Fermi energy, as shown in Figure 4(a), and the vHS below the Fermi energy has a particularly higher peak than that above the Fermi energy. These vHSs have the characters of localized Ru t_{2g} orbitals. According to the Stoner's theorem, if the structure is frozen as the intrinsic (undoped) case, hole doping and optical doping that also introduces holes shift the Fermi energy to vHSs with higher DOS and are more likely to induce the Stoner's instability than electron doping. This qualitatively explains why hole doping and optical doping favors the FM order even if we froze the structure at the intrinsic situation.

In addition to itinerant magnetism, the direct and indirect exchange couplings between localized moments of Ru³⁺ also affect the magnetic order of doped monolayer RuCl₃. This is particularly important for the case of electron doping. Rau et al.³³ proposed a generic spin model to study magnetic phase diagrams for materials with honeycomb layered structures similar to the A₂IrO₃ (A=Na, Li) family iridates and RuCl₃. We will employ this analytical model to analyze the couplings between

localized magnetic moments in carrier or optically doped monolayer RuCl₃. This spin model considers the Heisenberg interaction (J), Kitaev interaction (K), and symmetric off-diagonal exchange interaction (Γ) for the honeycomb lattice.

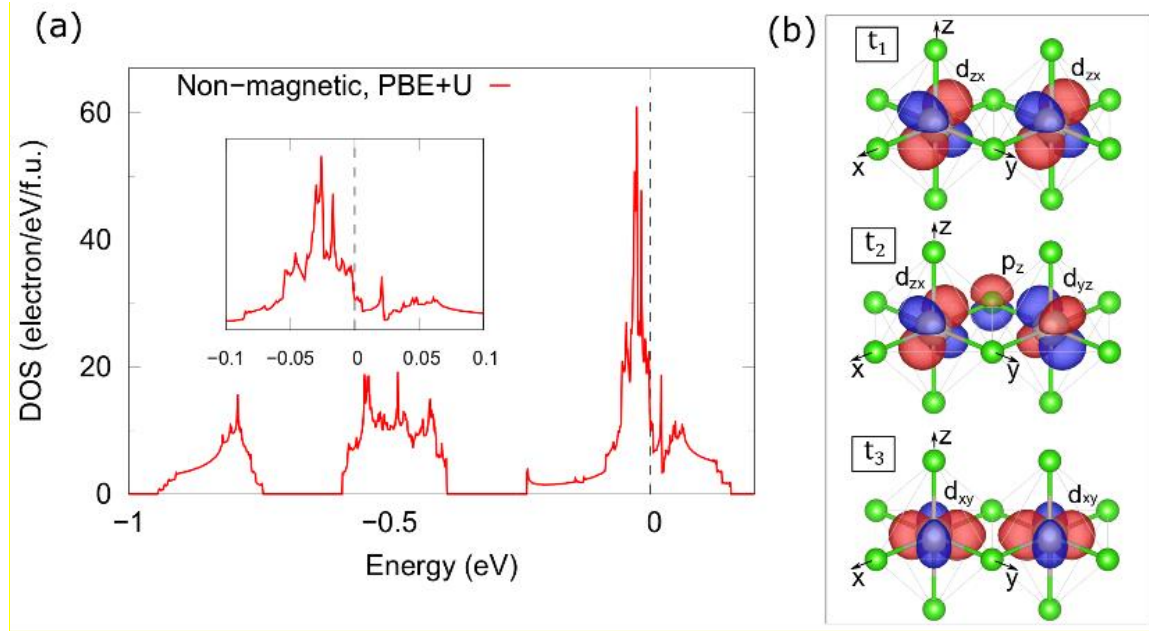


Figure 4 (a) Density of states (DOS) of intrinsic monolayer RuCl₃ in a non-magnetic state. This plot is calculated with the structure relaxed with the Zigzag AFM phase. Inset: the zoom-in plot of DOS near the Fermi energy. (b) Schematic plots of the hopping channels between t_{2g} orbitals.

These magnetic interactions (J, K, and Γ) are determined by three hopping integrals, denoted as t_1 , t_2 , and t_3 , between Ru t_{2g} orbitals, which was schematically plotted in Figure 4 (b). We construct the tight-binding Hamiltonian using maximally localized Wannier functions⁴⁸ for the t_{2g} orbitals of Ru atoms and obtain the hopping integrals t_i ($i=1,2,3$) from the tight-binding Hamiltonian. Then, we calculate the exchange parameters J, K, and Γ for a few different doping conditions, as shown in Table 1. Details on calculating hopping integrals and exchange parameters are presented in the Supporting Information.

Overall, we find the Heisenberg exchange J is ferromagnetic, while the Kitaev exchange K is antiferromagnetic. The magnitude of Kitaev interaction K is about twice the Heisenberg interaction J. The off-diagonal term Γ is ferromagnetic and smaller than K by an order of magnitude. According to the phase diagram of the generic spin model³³, the magnetic order of RuCl₃ is determined by the $\phi = \arctan(\frac{J}{K})$ and $\theta = \arctan(\frac{\sqrt{J^2+K^2}}{\Gamma})$, i.e., the ratio between J, K, and Γ . The intrinsic RuCl₃ has a zigzag AFM phase. As doping carriers change from holes to electrons, the parameter ϕ increases monotonically from 0.635π (hole doping) to 0.646π (electron doping), during which the structure is relaxed and, thus, the corresponding strain effect is included. This drives the system towards the FM phase. This qualitatively explains that electron-doping induces ferromagnetism through strain effects and variation of exchange couplings. Meanwhile, we must admit that, although the changing trend of ϕ qualitatively prefers the FM order, the variation value is smaller than the threshold value in Ref.³³. One reason can be that it is hard to get close quantitative agreements between models and first-principles calculations in correlated magnetic materials. Meanwhile, the electron-induced FM order benefits from both exchange interactions and itinerant magnetism.

Table 1. The exchange coupling constants calculated from tight-binding hopping parameters.

Doping density (f.u. ⁻¹)	J (meV)	K	Γ	ϕ	Θ
-0.075 (electron)	-4.69	9.47	-0.91	0.646π	0.527π
0.0	-5.31	11.46	-1.42	0.638π	0.536π
0.075 (hole)	-6.10	13.55	-1.92	0.635π	0.541π

2.5. Estimation of Curie temperature

To estimate the Curie temperature of the doping-induced FM phase, we fit the total energies of these four spin configurations with a 2D Ising model, including up to third nearest-neighbor (NN) exchange coupling, and extract the exchange coupling constants. In Figures 5 (a) and (b), we present the calculated exchange coupling constants under different doping densities. Under electron doping, the magnitude of the second NN exchange coupling J_2 and the third NN exchange coupling J_3 can be as large as 8 meV, which is comparable to the NN coupling J_1 . Interestingly, J_1 remains to be positive (i.e., supporting the FM order) under different doping conditions, and increases with the carrier concentration. Previous experimental works⁴⁹ also support that the coupling between NN Ru is FM.

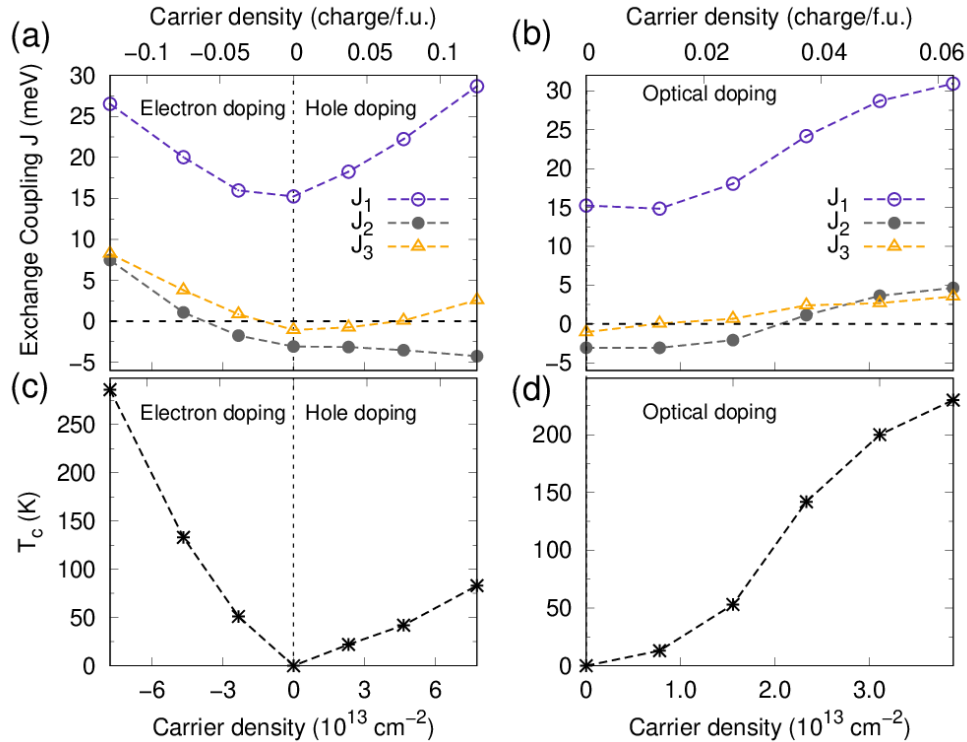


Figure 5 (a) and (b) The exchange coupling constants (J_1, J_2 , and J_3) according to the unipolar doping and optical e - h doping, respectively. (c) and (d) The MC simulated Curie temperature of monolayer RuCl₃ under the unipolar doping and optical e - h doping, respectively.

With the exchange coupling constants J_i ($i=1,2,3$) as inputs, we estimate the Curie temperature T_c of the doping-induced FM phases using Monte Carlo (MC) simulations based on the Metropolis algorithm. Figure

5 (c) and (d) show T_c for different doping densities. The estimated T_c can be significantly increased under doping with the provision that the Ising model is a rough estimation, which tends to overestimate the Curie temperature.

3. CONCLUSION

We performed first-principles calculations to investigate the ground-state of monolayer RuCl_3 under electrostatic and optical dopings. Our calculations show that an intrinsic monolayer RuCl_3 has nearly degenerate FM and zigzag AFM orders. This results and previous work both indicate that the undoped monolayer RuCl_3 shows signatures of strong magnetic frustrations and quantum spin liquid. We predict that electrostatic doping with either electrons or holes and optical doping can both cause a phase transition from the spin-liquid phase to the FM order with a moderate carrier/ e - h density, achievable with current experimental techniques. Increasing e - h pair density by optical doping can further enhance ferromagnetism and increases the Curie temperature significantly. The mechanisms for driving the magnetic phase transition are discussed based on changes of crystal structures and orbital components. In brief, electron doping drives the magnetic phase transition mainly by inducing a tensile strain, while hole doping and optical electron-hole doping enhances ferromagnetism by altering the occupations of Ru 4d t_{2g} orbitals and itinerant magnetism. Optically driving 2D ferromagnetism offers the possibility of non-contact tunability for exploring new physics and spintronic applications.

4. COMPUTATIONAL DETAILS

4.1. DFT calculations

We carry out pseudopotential DFT calculations with the plane-wave based Quantum Espresso code⁵⁰⁻⁵¹. The Perdew-Burke-Ernzerhof (PBE) functional⁵² is used in calculations. The ion core potentials (nuclei and core electrons) are described with optimized norm-conserving Vanderbilt pseudopotentials with scalar-relativistic effects, provided by the Pseudo Dojo project⁵³. Semi-core 4s and 4p electrons of Ru are explicitly treated as valence electrons. Since Ru has moderate spin-orbit effects, we also did calculations for unipolar doping cases using VASP⁵⁴⁻⁵⁶ with full relativistic effects and our main conclusions are not changed (as shown in Supporting Information).

Following previous work^{31,34}, an effective Hubbard $U_{\text{eff}}=U-J=2.0$ eV is used. We notice the Hubbard U_{eff} used in previous work ranges from 1.5 eV to 3.0 eV^{29,57}. An experimental study suggests that $U=2.4$ eV and $J=0.4$ eV are reasonable guesses⁵⁸. The dependence of our results on U_{eff} is studied and presented in Supporting Information.

The k -grids of $6\times 3\times 1$ and $15\times 8\times 1$ are used for the Brillouin-zone sampling in intrinsic and doped cases, respectively. We set the distance d between neighboring layers as 15 Angstrom to avoid spurious interactions. For structural optimizations, we relax both the atomic coordinates and the lattice constants so that residue forces are less than 2×10^{-4} Ry/a.u. and total energies are converged within 1×10^{-4} Ry. Due to the strong magnetic frustration²⁸, there are many competing magnetic phases of monolayer RuCl_3 . Even though these local minima phases may have the same total magnetization, the local distributions of spin polarization can be different and result in slightly different relaxed structures and total energies. We have performed structural relaxations with different starting points to find the structure with the lowest energy.

We constructed Maximally Localized Wannier Functions (MLWF) for the Cl p orbitals and Ru t_{2g} orbitals using the Wannier90 package⁵⁹⁻⁶⁰. The hopping integrals between Ru t_{2g} orbitals is obtained from the tight-binding Hamiltonian built with MLWF.

Finally, we must point out that the first-principles simulations of correlated magnetic materials, in particular for the highly frustrated system like RuCl₃, are affected by the choice of functionals, pseudopotentials, effective Hubbard term U_{eff} , and spin-orbit coupling (SOC). In Supporting Information, we discussed their impacts and find that these factors can affect our results quantitatively. For example, the relative energies calculated by different exchange-correlation functionals can differ by 6 meV/f.u. Nevertheless, our main conclusions, i.e., the enhancement of ferromagnetism under doping conditions, still holds (see Supporting Information section 1).

4.2. Ising model and MC simulations

We extract the exchange coupling constants up to the third-nearest neighbor by mapping the total energies of monolayer RuCl₃ of four different magnetic orders to the Ising model on 2D hexagonal lattices

$$H = -\frac{1}{2} \left(\sum_{\langle i,j \rangle} J_1 S_i S_j + \sum_{\langle\langle i,j \rangle\rangle} J_2 S_i S_j + \sum_{\langle\langle\langle i,j \rangle\rangle\rangle} J_3 S_i S_j \right)$$

where $S_{1,2} = \pm 1/2$ and J_1, J_2 , and J_3 correspond to exchange coupling constants between the NN, second NN, and third NN couplings.

With the Ising model, the exchange energies for four magnetic phases are given by:

$$\begin{aligned} E_{FM} &= \frac{1}{4} (-6J_1 - 12J_2 - 6J_3) \\ E_{ZZAFM} &= \frac{1}{4} (-2J_1 + 4J_2 + 6J_3) \\ E_{Neel} &= \frac{1}{4} (6J_1 - 12J_2 + 6J_3) \\ E_{stripy} &= \frac{1}{4} (2J_1 + 4J_2 - 6J_3) \end{aligned}$$

For the MC simulation, we employ a hexagonal lattice with 60×60 spin sites, which is large enough to eliminate finite-size effects. To converge the canonical ensemble average magnetization, we ran the simulation with 1.3×10^5 Monte Carlo steps for each temperature points. We provide results of MC simulations for several doping densities in Supporting Information.

Author information

Corresponding Author

James R. Chelikowsky: jrc@utexas.edu

Li Yang: lyang@physics.wustl.edu

Author Contributions

Y. T. and W. G. contributed equally to this work.

Acknowledgement

We thank Dr. Yan Lyu and Dr. Ruixiang Fei for their helpful discussion. YT and LY are supported by the National Science Foundation (NSF) CAREER Grant No. DMR-1455346 and the Air Force Office of Scientific Research (AFOSR) grant No. FA9550-17-1-0304. EAH acknowledges support under NSF DMR-1810305. Work at the University of Texas at Austin was supported from a subaward from the Center for Computational Study of Excited-State Phenomena in Energy Materials at the Lawrence Berkeley National Laboratory, which is funded by the U.S. Department of Energy, Office of Science, Basic Energy Sciences, Materials Sciences and Engineering Division under Contract No. DEAC0205CH11231, as part of the Computational Materials Sciences Program. Computational resources are provided by the Texas Advanced Computing Center (TACC).

Reference

1. Ma, Y.; Dai, Y.; Guo, M.; Niu, C.; Zhu, Y.; Huang, B., Evidence of the Existence of Magnetism in Pristine VX ₂ Monolayers (X = S, Se) and Their Strain-Induced Tunable Magnetic Properties. *ACS Nano* **2012**, *6*, 1695-1701.
2. Zhou, Y.; Wang, Z.; Yang, P.; Zu, X.; Yang, L.; Sun, X.; Gao, F., Tensile Strain Switched Ferromagnetism in Layered NbS₂ and NbSe₂. *ACS Nano* **2012**, *6*, 9727-9736.
3. Yazyev, O. V., Emergence of magnetism in graphene materials and nanostructures. *Reports on Progress in Physics* **2010**, *73*, 056501.
4. Han, W.; Kawakami, R. K.; Gmitra, M.; Fabian, J., Graphene spintronics. *Nature Nanotechnology* **2014**, *9*, 794-807.
5. Haugen, H.; Huertas-Hernando, D.; Brataas, A., Spin transport in proximity-induced ferromagnetic graphene. *Physical Review B* **2008**, *77*, 115406.
6. Huang, B.; Clark, G.; Navarro-Moratalla, E.; Klein, D. R.; Cheng, R.; Seyler, K. L.; Zhong, D.; Schmidgall, E.; McGuire, M. A.; Cobden, D. H.; Yao, W.; Xiao, D.; Jarillo-Herrero, P.; Xu, X., Layer-dependent ferromagnetism in a van der Waals crystal down to the monolayer limit. *Nature* **2017**, *546*, 270-273.
7. Gong, C.; Li, L.; Li, Z.; Ji, H.; Stern, A.; Xia, Y.; Cao, T.; Bao, W.; Wang, C.; Wang, Y.; Qiu, Z. Q.; Cava, R. J.; Louie, S. G.; Xia, J.; Zhang, X., Discovery of intrinsic ferromagnetism in two-dimensional van der Waals crystals. *Nature* **2017**, *546*, 265-269.
8. Lin, M.-W.; Zhuang, H. L.; Yan, J.; Ward, T. Z.; Poretzky, A. A.; Rouleau, C. M.; Gai, Z.; Liang, L.; Meunier, V.; Sumpter, B. G.; Ganesh, P.; Kent, P. R. C.; Geohegan, D. B.; Mandrus, D. G.; Xiao, K., Ultrathin nanosheets of CrSiTe₃: a semiconducting two-dimensional ferromagnetic material. *Journal of Materials Chemistry C* **2016**, *4*, 315-322.
9. Bonilla, M.; Kolekar, S.; Ma, Y.; Diaz, H. C.; Kalappattil, V.; Das, R.; Eggers, T.; Gutierrez, H. R.; Phan, M.-H.; Batzill, M., Strong room-temperature ferromagnetism in VSe₂ monolayers on van der Waals substrates. *Nature Nanotechnology* **2018**, *13*, 289-293.
10. Deng, Y.; Yu, Y.; Song, Y.; Zhang, J.; Wang, N. Z.; Sun, Z.; Yi, Y.; Wu, Y. Z.; Wu, S.; Zhu, J.; Wang, J.; Chen, X. H.; Zhang, Y., Gate-tunable room-temperature ferromagnetism in two-dimensional Fe₃GeTe₂. *Nature* **2018**, *563*, 94-99.
11. O'Hara, D. J.; Zhu, T.; Trout, A. H.; Ahmed, A. S.; Luo, Y. K.; Lee, C. H.; Brenner, M. R.; Rajan, S.; Gupta, J. A.; McComb, D. W.; Kawakami, R. K., Room Temperature Intrinsic Ferromagnetism in Epitaxial Manganese Selenide Films in the Monolayer Limit. *Nano Letters* **2018**, *18*, 3125-3131.
12. Gong, C.; Zhang, X., Two-dimensional magnetic crystals and emergent heterostructure devices. *Science* **2019**, *363*, eaav4450.
13. Jiang, S.; Li, L.; Wang, Z.; Shan, J.; Mak, K. F., Spin transistor built on 2D van der Waals heterostructures. *Arxiv* **2018**.
14. Huang, B.; Clark, G.; Klein, D. R.; MacNeill, D.; Navarro-Moratalla, E.; Seyler, K. L.; Wilson, N.; McGuire, M. A.; Cobden, D. H.; Xiao, D.; Yao, W.; Jarillo-Herrero, P.; Xu, X., Electrical control of 2D magnetism in bilayer CrI₃. *Nature Nanotechnology* **2018**, *13*, 544-548.
15. Jiang, S.; Li, L.; Wang, Z.; Mak, K. F.; Shan, J., Controlling magnetism in 2D CrI₃ by electrostatic doping. *Nature Nanotechnology* **2018**, *13*, 549-553.
16. Britnell, L.; Ribeiro, R. M.; Eckmann, A.; Jalil, R.; Belle, B. D.; Mishchenko, A.; Kim, Y.-J.; Gorbachev, R. V.; Georgiou, T.; Morozov, S. V.; Grigorenko, A. N.; Geim, A. K.; Casiraghi, C.; Neto, A. H. C.; Novoselov, K. S., Strong Light-Matter Interactions in Heterostructures of Atomically Thin Films. *Science* **2013**, *340*, 1311-1314.
17. Bernardi, M.; Palummo, M.; Grossman, J. C., Extraordinary Sunlight Absorption and One Nanometer Thick Photovoltaics Using Two-Dimensional Monolayer Materials. *Nano Letters* **2013**, *13*, 3664-3670.

18. Lysenko, S.; Rua, A. J.; Vikhnin, V.; Jimenez, J.; Fernandez, F.; Liu, H., Light-induced ultrafast phase transitions in VO₂ thin film. *Applied Surface Science* **2006**, *252*, 5512-5515.
19. Hilton, D. J.; Prasankumar, R. P.; Fourmaux, S.; Cavalleri, A.; Brassard, D.; El Khakani, M. A.; Kieffer, J. C.; Taylor, A. J.; Averitt, R. D., Enhanced Photosusceptibility near T_c for the Light-Induced Insulator-to-Metal Phase Transition in Vanadium Dioxide. *Physical Review Letters* **2007**, *99*, 226401.
20. Yuan, X.; Zhang, W.; Zhang, P., Hole-lattice coupling and photoinduced insulator-metal transition in VO₂. *Physical Review B* **2013**, *88*, 035119.
21. Náfrádi, B.; Szirmai, P.; Spina, M.; Lee, H.; Yazyev, O. V.; Arakcheeva, A.; Chernyshov, D.; Gibert, M.; Forró, L.; Horváth, E., Optically switched magnetism in photovoltaic perovskite CH₃NH₃(Mn:Pb)I₃. *Nature Communications* **2016**, *7*, 13406.
22. Kimel, A. V.; Kirilyuk, A.; Tsvetkov, A.; Pisarev, R. V.; Rasing, T., Laser-induced ultrafast spin reorientation in the antiferromagnet TmFeO₃. *Nature* **2004**, *429* (6994), 850-853.
23. Vahaplar, K.; Kalashnikova, A. M.; Kimel, A. V.; Hinzke, D.; Nowak, U.; Chantrell, R.; Tsukamoto, A.; Itoh, A.; Kirilyuk, A.; Rasing, T., Ultrafast Path for Optical Magnetization Reversal via a Strongly Nonequilibrium State. *Physical Review Letters* **2009**, *103* (11), 117201.
24. Fausti, D.; Tobey, R. I.; Dean, N.; Kaiser, S.; Dienst, A.; Hoffmann, M. C.; Pyon, S.; Takayama, T.; Takagi, H.; Cavalleri, A., Light-Induced Superconductivity in a Stripe-Ordered Cuprate. *Science* **2011**, *331*, 189-191.
25. Haleoot, R.; Paillard, C.; Kaloni, T. P.; Mehboudi, M.; Xu, B.; Bellaiche, L.; Barraza-Lopez, S., Photostrictive Two-Dimensional Materials in the Monochalcogenide Family. *Physical Review Letters* **2017**, *118*, 227401.
26. Zhou, B.; Wang, Y.; Osterhoudt, G. B.; Lampen-Kelley, P.; Mandrus, D.; He, R.; Burch, K. S.; Henriksen, E. A., Possible structural transformation and enhanced magnetic fluctuations in exfoliated α -RuCl₃. *Journal of Physics and Chemistry of Solids* **2018**.
27. Mashhadi, S.; Weber, D.; Schoop, L. M.; Schulz, A.; Lotsch, B. V.; Burghard, M.; Kern, K., Electrical Transport Signature of the Magnetic Fluctuation-Structure Relation in α -RuCl₃ Nanoflakes. *Nano Letters* **2018**, *18*, 3203-3208.
28. Du, L.; Huang, Y.; Wang, Y.; Wang, Q.; Yang, R.; Tang, J.; Liao, M.; Shi, D.; Shi, Y.; Zhou, X.; Zhang, Q.; Zhang, G., 2D proximate quantum spin liquid state in atomic-thin α -RuCl₃. *2D Materials* **2018**, *6* (1), 015014.
29. Johnson, R. D.; Williams, S. C.; Haghighirad, A. A.; Singleton, J.; Zapf, V.; Manuel, P.; Mazin, I. I.; Li, Y.; Jeschke, H. O.; Valentí, R.; Coldea, R., Monoclinic crystal structure of α -RuCl₃ and the zigzag antiferromagnetic ground state. *Physical Review B* **2015**, *92*, 235119.
30. Sandilands, L. J.; Tian, Y.; Plumb, K. W.; Kim, Y.-J.; Burch, K. S., Scattering Continuum and Possible Fractionalized Excitations in α -RuCl₃. *Physical Review Letters* **2015**, *114*, 147201.
31. Kim, H.-S.; Kee, H.-Y., Crystal structure and magnetism in α -RuCl₃: An *ab initio* study. *Physical Review B* **2016**, *93*, 155143.
32. Mermin, N. D.; Wagner, H., Absence of Ferromagnetism or Antiferromagnetism in One- or Two-Dimensional Isotropic Heisenberg Models. *Physical Review Letters* **1966**, *17*, 1133-1136.
33. Rau, J. G.; Lee, E. K.-H.; Kee, H.-Y., Generic Spin Model for the Honeycomb Iridates beyond the Kitaev Limit. *Physical Review Letters* **2014**, *112*, 077204.
34. Iyikanat, F.; Yagmurcukardes, M.; Senger, R. T.; Sahin, H., Tuning electronic and magnetic properties of monolayer α -RuCl₃ by in-plane strain. *Journal of Materials Chemistry C* **2018**, *6*, 2019-2025.
35. Sarikurt, S.; Kadioglu, Y.; Ersan, F.; Vatansever, E.; Aktürk, O. Ü.; Yüksel, Y.; Akıncı, Ü.; Aktürk, E., Electronic and magnetic properties of monolayer α -RuCl₃: a first-principles and Monte Carlo study. *Physical Chemistry Chemical Physics* **2018**, *20* (2), 997-1004.
36. Cao, T.; Li, Z.; Louie, S. G., Tunable Magnetism and Half-Metallicity in Hole-Doped Monolayer GaSe. *Physical Review Letters* **2015**, *114*, 236602.

37. Li, X.; Wu, X.; Yang, J., Half-Metallicity in MnPSe ₃ Exfoliated Nanosheet with Carrier Doping. *Journal of the American Chemical Society* **2014**, *136*, 11065-11069.
38. Liu, J.; Sun, Q.; Kawazoe, Y.; Jena, P., Exfoliating biocompatible ferromagnetic Cr-trihalide monolayers. *Physical Chemistry Chemical Physics* **2016**, *18*, 8777-8784.
39. Tiberj, A.; Rubio-Roy, M.; Paillet, M.; Huntzinger, J.-R.; Landois, P.; Mikolasek, M.; Contreras, S.; Sauvajol, J.-L.; Dujardin, E.; Zahab, A.-A., Reversible optical doping of graphene. *Scientific Reports* **2013**, *3*, 2355.
40. Han, T.-R. T.; Zhou, F.; Malliakas, C. D.; Duxbury, P. M.; Mahanti, S. D.; Kanatzidis, M. G.; Ruan, C.-Y., Exploration of metastability and hidden phases in correlated electron crystals visualized by femtosecond optical doping and electron crystallography. *Science Advances* **2015**, *1*, e1400173.
41. Chernikov, A.; Ruppert, C.; Hill, H. M.; Rigosi, A. F.; Heinz, T. F., Population inversion and giant bandgap renormalization in atomically thin WS₂ layers. *Nature Photonics* **2015**, *9*, 466-470.
42. Abtew, T. A.; Sun, Y. Y.; Shih, B.-C.; Dev, P.; Zhang, S. B.; Zhang, P., Dynamic Jahn-Teller Effect in the $\text{NV}^{\text{center}}$ in Diamond. *Physical Review Letters* **2011**, *107* (14), 146403.
43. Dreyer, C. E.; Alkauskas, A.; Lyons, J. L.; Janotti, A.; Walle, C. G. V. d., First-Principles Calculations of Point Defects for Quantum Technologies. *Annual Review of Materials Research* **2018**, *48* (1), 1-26.
44. Paillard, C.; Xu, B.; Dkhil, B.; Geneste, G.; Bellaiche, L., Photostriction in Ferroelectrics from Density Functional Theory. *Physical Review Letters* **2016**, *116* (24), 247401-247401.
45. Wang, H.; Zhang, C.; Rana, F., Ultrafast Dynamics of Defect-Assisted Electron-Hole Recombination in Monolayer MoS₂. *Nano Letters* **2015**, *15*, 339-345.
46. Beaurepaire, E.; Merle, J. C.; Daunois, A.; Bigot, J. Y., Ultrafast Spin Dynamics in Ferromagnetic Nickel. *Physical Review Letters* **1996**, *76* (22), 4250-4253.
47. Zhang, G. P.; Hübner, W.; Lefkidis, G.; Bai, Y.; George, T. F., Paradigm of the time-resolved magneto-optical Kerr effect for femtosecond magnetism. *Nature Physics* **2009**, *5*, 499.
48. Marzari, N.; Mostofi, A. A.; Yates, J. R.; Souza, I.; Vanderbilt, D., Maximally localized Wannier functions: Theory and applications. *Reviews of Modern Physics* **2012**, *84* (4), 1419-1475.
49. Plumb, K. W.; Clancy, J. P.; Sandilands, L. J.; Shankar, V. V.; Hu, Y. F.; Burch, K. S.; Kee, H.-Y.; Kim, Y.-J., $\alpha\text{-RuCl}_3$: A spin-orbit assisted Mott insulator on a honeycomb lattice. *Physical Review B* **2014**, *90* (4), 041112.
50. Giannozzi, P.; Baroni, S.; Bonini, N.; Calandra, M.; Car, R.; Cavazzoni, C.; Ceresoli, D.; Chiarotti, G. L.; Cococcioni, M.; Dabo, I.; Dal Corso, A.; de Gironcoli, S.; Fabris, S.; Fratesi, G.; Gebauer, R.; Gerstmann, U.; Gougoussis, C.; Kokalj, A.; Lazzeri, M.; Martin-Samos, L.; Marzari, N.; Mauri, F.; Mazzarello, R.; Paolini, S.; Pasquarello, A.; Paulatto, L.; Sbraccia, C.; Scandolo, S.; Sclauzero, G.; Seitsonen, A. P.; Smogunov, A.; Umari, P.; Wentzcovitch, R. M., QUANTUM ESPRESSO: a modular and open-source software project for quantum simulations of materials. *Journal of Physics: Condensed Matter* **2009**, *21*, 395502.
51. Giannozzi, P.; Andreussi, O.; Brumme, T.; Bunau, O.; Buongiorno Nardelli, M.; Calandra, M.; Car, R.; Cavazzoni, C.; Ceresoli, D.; Cococcioni, M.; Colonna, N.; Carnimeo, I.; Dal Corso, A.; de Gironcoli, S.; Delugas, P.; DiStasio, R. A.; Ferretti, A.; Floris, A.; Fratesi, G.; Fugallo, G.; Gebauer, R.; Gerstmann, U.; Giustino, F.; Gorni, T.; Jia, J.; Kawamura, M.; Ko, H.-Y.; Kokalj, A.; Küçükbenli, E.; Lazzeri, M.; Marsili, M.; Marzari, N.; Mauri, F.; Nguyen, N. L.; Nguyen, H.-V.; Otero-de-la-Roza, A.; Paulatto, L.; Poncé, S.; Rocca, D.; Sabatini, R.; Santra, B.; Schlipf, M.; Seitsonen, A. P.; Smogunov, A.; Timrov, I.; Thonhauser, T.; Umari, P.; Vast, N.; Wu, X.; Baroni, S., Advanced capabilities for materials modelling with Quantum ESPRESSO. *Journal of Physics: Condensed Matter* **2017**, *29*, 465901.
52. Perdew, J. P.; Burke, K.; Ernzerhof, M., Generalized Gradient Approximation Made Simple. *Physical Review Letters* **1996**, *77* (18), 3865-3868.

53. van Setten, M. J.; Giantomassi, M.; Bousquet, E.; Verstraete, M. J.; Hamann, D. R.; Gonze, X.; Rignanese, G.-M., The PseudoDojo: Training and grading a 85 element optimized norm-conserving pseudopotential table. *Computer Physics Communications* **2018**, *226*, 39-54.
54. Kresse, G.; Furthmüller, J., Efficiency of ab-initio total energy calculations for metals and semiconductors using a plane-wave basis set. *Computational Materials Science* **1996**, *6* (1), 15-50.
55. Kresse, G.; Furthmüller, J., Efficient iterative schemes for ab initio total-energy calculations using a plane-wave basis set. *Physical Review B* **1996**, *54* (16), 11169-11186.
56. Kresse, G.; Joubert, D., From ultrasoft pseudopotentials to the projector augmented-wave method. *Physical Review B* **1999**, *59* (3), 1758-1775.
57. Kim, H.-S.; V., V. S.; Catuneanu, A.; Kee, H.-Y., Kitaev magnetism in honeycomb RuCl_3 with intermediate spin-orbit coupling. *Physical Review B* **2015**, *91*, 241110.
58. Sandilands, L. J.; Tian, Y.; Reijnders, A. A.; Kim, H.-S.; Plumb, K. W.; Kim, Y.-J.; Kee, H.-Y.; Burch, K. S., Spin-orbit excitations and electronic structure of the putative Kitaev magnet $\alpha\text{-RuCl}_3$. *Physical Review B* **2016**, *93* (7), 075144.
59. Mostofi, A. A.; Yates, J. R.; Lee, Y.-S.; Souza, I.; Vanderbilt, D.; Marzari, N., wannier90: A tool for obtaining maximally-localised Wannier functions. *Computer Physics Communications* **2008**, *178* (9), 685-699.
60. Mostofi, A. A.; Yates, J. R.; Pizzi, G.; Lee, Y.-S.; Souza, I.; Vanderbilt, D.; Marzari, N., An updated version of wannier90: A tool for obtaining maximally-localised Wannier functions. *Computer Physics Communications* **2014**, *185* (8), 2309-2310.